An Experimental and Theoretical Study of the Electronic Structure of Zinc Thiophenolate-Capped Clusters

Renzo Bertoncello,[†] Marco Bettinelli,[‡] Maurizio Casarin,*[,†] Chiara Maccato,[†] Luciano Pandolfo,[†] and Andrea Vittadini[§]

Dipartimento C.I.M.A., Università di Padova, Via Loredan 4, 35131 Padova, Italy, Istituto Policattedra, Università di Verona, Strada Le Grazie, 37134 Verona, Italy, and I.C.T.I.M.A., CNR, Corso Stati Uniti 4, 35020 Padova, Italy

Received February 12, 1997[⊗]

The electronic structure of a series of thiophenolate-capped ionic/neutral clusters ($[Zn(SPh)_4]^{2-}$ (**1**); $[Zn_4(\mu_2\text{-}SPh)_6(SPh)_4]^{2-}$ (**2**); $Zn_{10}(\mu_3\text{-}S)_4(\mu_2\text{-}SPh)_{12}$ (**3**); and $[Zn_{10}(\mu_3\text{-}S)_4(\mu_2\text{-}SPh)_{12}(SPh)_4]^{4-}$ (**4**), Ph = phenyl), indicated as supertetrahedral fragments and possible molecular models of cubic ZnS, has been investigated by coupling density functional calculations to UV electronic and X-ray photoelectron (XP) spectroscopy. Theoretical outcomes indicate that, on passing from the tetrametallic to the decametallic clusters, there is a modification in the nature of the outermost occupied and lowermost unoccupied molecular orbitals. Actually, both in **1** and in **2** the frontier orbitals are delocalized and mainly composed of the S 3p pairs strongly mixed with the Ph π levels (the HOMOs) and of the linear combinations of Ph π^* orbitals, the LUMOs. At variance to that, in **3** and **4** both the HOMO and LUMO are highly localized, the former on μ_3-S atoms occupying C_{3v} coordinatively unsaturated tetrahedral positions and the latter on peripheral Zn atoms. The nature of the electronic levels involved in the UV absorption bands is discussed, and the agreement between theory and experiment is satisfactory. Neither experimental nor theoretical electronic excitation energies are influenced by the cluster size. Moreover, XPS data match quite well variations of the Zn and S gross atomic charges along the series. The different Zn−S bonding scheme characterizing terminal, μ_2-bridging, and μ_3-pyramidal S atoms allows a rationalization of the cluster behavior in solution. Along the investigated series, the only species reasonably mimicking both the structural arrangement and the electronic structure of the solid ZnS is $Zn_{10}(\mu_3\text{-}S)_4(\mu_2\text{-}SPh)_{12}$, which can be considered a molecular model of ZnS nonpolar surfaces.

1. Introduction

Ultrasmall particles of semiconductors represent an outstanding new class of materials.[1] These particles, also named clusters, quantum dots, nanocrystals, Q-particles, etc., have dimensions ranging from a few to hundreds of angstroms and electronic properties in between those of the solid and those of molecular systems. Interestingly, many of these particles contain all of the structural features of the solid while remaining soluble in organic solvents, retaining in this sense the appealing properties of discrete molecules. Moreover, these particles are attractive not only for their nonlinear optical properties[2] but also because they can be used as building blocks in the preparation of new materials not obtainable through traditional techniques.[3] In this context, one of the most important results has certainly been the synthesis, crystallization, and structural characterization of a series of metal chalcogenides having thiolate (in particular thiophenolate) capping ligands such as $(Me_4N)_2[M(SPh)_4]$ (Me = methyl; Ph = phenyl; M = Cd, Zn),[3] $(Me_4N)_2[M_4(\mu_2\text{-}SPh)_6(SPh)_4]$,[3] $[Zn(SEt)Et]_{10}$ (Et = ethyl),[4] $M_{10}(\mu_3\text{-}S)_4(\mu_2\text{-}SR)_{12}$ (M = Zn and R = Et,[5] M = Zn, Cd and R = Ph[6]), $(Me_4N)_4[M_{10}(\mu_3\text{-}E)_4(\mu_2\text{-}SPh)_{12}(SPh)_4]$ (E = S, Se),[3] $Cd_{17}(\mu_4\text{-}S)_4(\mu_2\text{-}SR)_{26}$ (R = CH_2CH_2OH),[7] $(Me_4N)_2[Cd_{17}(\mu_4\text{-}S)_4(\mu_2\text{-}SPh)_{24}(SPh)_4]$,[8] $[Cd_{20}(\mu_4\text{-}S)(\mu_3\text{-}S)_{12}(\mu_2\text{-}SPh)_{18}(SPh)_4]^{8-}$,[9] and $Cd_{32}(\mu_4\text{-}S)_{10}(\mu_3\text{-}S)_4(\mu_2\text{-}SR)_{36}\cdot 4L$ (R = Ph,[10] $CH_2CH(OH)CH_3$;[11] L = DMF,[10] H_2O[11]). Furthermore, the thermal decomposition of the neutral Zn and Cd clusters at temperatures well below 500 °C can be considered an alternative route to synthesize amorphous ZnS and CdS,[4,8,12] even though it has been shown recently that amorphous zinc and cadmium sulfides can be obtained at room temperature (RT) through the reaction of elemental metals with sulfur in liquid ammonia.[13] Such a huge experimental effort has been so far accompanied by few theoretical investigations mainly focused on Cd derivatives.[9,14−16] Moreover, peripheral ligands have been included only in one case,[16] while their influence on the

* Author to whom correspondence should be addressed. Phone: 39-49-8275164. Fax: 39-49-8275161. E−mail: casarin@chim02.unipd.it.
† Dipartimento CIMA, Università di Padova.
‡ Istituto Policattedra, Università di Verona.
§ ICTIMA, CNR di Padova.
⊗ Abstract published in *Advance ACS Abstracts,* September 1, 1997.

(1) (a) Wang, Y.; Herron, N. *J. Phys. Chem.* **1991**, *95*, 525; (b) Weller, H. *Angew. Chem., Int. Ed. Engl.* **1993**, *32*, 41.
(2) (a) Wang, Y.; Herron, N.; Mahler, W.; Suna, A. *J. Opt. Soc. Am. B* **1989**, *6*, 808. (b) Wang, Y.; Mahler, W. *Opt. Commun.* **1987**, *61*, 233. (c) Hilinski, E.; Lucas, P.; Wang, Y. *J. Chem. Phys.* **1988**, *89*, 3435. (d) Wang, Y.; Suna, A.; McHugh, J.; Hilinski, E.; Lucas, P.; Johnson, R. D. *J. Chem. Phys.* **1990**, *92*, 6927.
(3) Dance, I. G.; Choy, A.; Scudder, M. L. *J. Am. Chem. Soc.* **1984**, *106*, 6285.
(4) Zeng, D.; Hampden-Smith, M. J.; Duesler, E. N. *Inorg. Chem.* **1994**, *33*, 5376.
(5) Nyman, M. D.; Hampden-Smith, M. J.; Duesler, E. N. *Inorg. Chem.* **1996**, *35*, 802.
(6) Farneth, W. E.; Herron, N.; Wang, Y. *Chem. Mater.* **1992**, *4*, 916.
(7) Vossmeyer, T.; Reck, G.; Katsikas, L.; Haupt, E. T. K.; Schulz, B.; Weller, H. *Science* **1995**, *267*, 1476.
(8) Lee, G. S. H.; Craig, D. C.; Ma, I.; Scudder, M. L.; Bailey, T. D.; Dance, I. G. *J. Am. Chem. Soc.* **1988**, *110*, 4863.
(9) Herron, N.; Suna, A.; Wang, Y. *J. Chem. Soc., Dalton Trans.* **1992**, 2329.
(10) Herron, N.; Calabrese, J. C.; Farneth, W. E.; Wang, Y. *Science* **1993**, *259*, 1426.
(11) Vossmeyer, T.; Reck, G.; Schulz, B.; Katsikas, L.; Weller, H. *J. Am. Chem. Soc.* **1995**, *117*, 12881.
(12) Casarin, M.; Maccato, C.; Pandolfo, L.; Vittadini, A. Manuscript in preparation.
(13) Henshaw, G.; Parkin, I. P.; Shaw, G. *Chem. Commun.* **1996**, 1095.
(14) Gurin, V. S. *J. Phys. Chem.* **1996**, *100*, 869.

S0020-1669(97)00165-1 CCC: $14.00

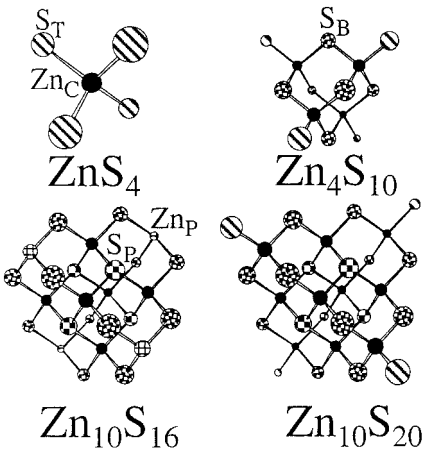

Figure 1. Ball and stick representations of $[Zn(SPh)_4]^{2-}$ (**1**), $[Zn_4(\mu_2\text{-}SPh)_6(SPh)_4]^{2-}$ (**2**), $Zn_{10}(\mu_3\text{-}S)_4(\mu_2\text{-}SPh)_{12}$ (**3**), and $[Zn_{10}(\mu_3\text{-}S)_4(\mu_2\text{-}SPh)_{12}(SPh)_4]^{4-}$ (**4**) skeletons.

cluster electronic properties has been experimentally demonstrated.[10,11] Actually, spectral pattern differences of $Cd_{32}(\mu_4\text{-}S)_{10}(\mu_3\text{-}S)_4(\mu_2\text{-}SPh)_{36}\cdot 4DMF$ and $Cd_{32}(\mu_4\text{-}S)_{10}(\mu_3\text{-}S)_4(\mu_2\text{-}SCH_2\text{-}CH(OH)CH_3)_{36}\cdot 4H_2O$ have been ascribed to the different nature of peripheral ligands on terminal (T) and μ_2-bridging (B) S atoms as we find here for $Zn_{10}(\mu_3\text{-}S)_4(\mu_2\text{-}SEt)_{12}$[5] and $Zn_{10}(\mu_3\text{-}S)_4(\mu_2\text{-}SPh)_{12}$ (see below). Such a fact indicates that identical cluster skeletons do not necessarily imply equivalent cluster electronic properties; consequently, the suitability of the examined systems to be molecular models[17] of the extended solid has to be verified for each single case.

Some of us have used extensively in the recent past the molecular-cluster approach coupled to the density functional theory (DFT) to investigate localized phenomena in the solid state.[18] In particular, two small polynuclear clusters ($Zn_4(\mu_4\text{-}O)(O_2CR)_6$, R = Me[18a] and NEt_2[18b]), characterized by a central O tetrahedrally coordinated to four Zn atoms placed at the center of a tetrahedron of O atoms, were shown to be well-tailored molecular models of the solid ZnO. The study of molecular models of covalent/ionic solids is interesting not only to provide insights about properties of the solid itself but also to verify the ability of the molecular-cluster approach[19] to model extended systems.

In this contribution we present the first *ab initio* study of the electronic structure of a series of thiophenolate-capped ZnS ionic/neutral clusters: $[Zn(SPh)_4]^{2-}$ (**1**), $[Zn_4(\mu_2\text{-}SPh)_6(SPh)_4]^{2-}$ (**2**), $Zn_{10}(\mu_3\text{-}S)_4(\mu_2\text{-}SPh)_{12}$ (**3**), and $[Zn_{10}(\mu_3\text{-}S)_4(\mu_2\text{-}SPh)_{12}(SPh)_4]^{4-}$ (**4**) (Figure 1). The theoretical results are compared with experimental measurements based on UV electronic and X-ray photoelectron (XP) spectroscopy. The aims of this study are (i) to understand the role played by different organic fragments on terminal and μ_2-bridging S atoms in determining different UV absorption patterns and (ii) to test the possibility, suggested by the cluster stereochemistry, that some of the investigated molecules/ions could be considered molecular models of ZnS.

(15) Han, J.-G.; Li, J.-Q.; He, T.-J.; Liu, F.-C.; Zhang, Y.-W. *J. Mol. Struct. (THEOCHEM)* **1995**, *331*, 249.
(16) Liu, H.-J.; Hupp, J. T.; Ratner, M. A. *J. Phys. Chem.* **1996**, *100*, 12204.
(17) A molecular model of a solid is a molecule or ion whose stereochemistry and electronic structure reasonably mimic the structural arrangement and the nature of the valence (conduction) band top (bottom) of the solid itself.
(18) (a) Bertoncello, R.; Bettinelli, M.; Casarin, M.; Gulino, A.; Tondello, E.; Vittadini, A. *Inorg. Chem.* **1992**, *31*, 1558. (b) Casarin, M.; Tondello, E.; Calderazzo, F.; Vittadini, A.; Bettinelli, M.; Gulino, A. *J. Chem. Soc., Faraday Trans.* **1993**, *89*, 4363.
(19) Messmer, R. P. *Theory Chemisorpt.* **1977**, *8*, 215.

2. Experimental and Computational Details

2.1. Instrumentation, Materials, and Syntheses. All reactions and manipulations were carried out under an atmosphere of argon with standard Schlenk techniques. All solvents were distilled and degassed before use. PhSH, Et_3N, Me_4NCl, $ZnNO_3\cdot 6H_2O$, and S (Fluka) were used without further purification. $(Me_4N)_2[Zn(SPh)_4]$, $(Me_4N)_2[Zn_4(\mu_2\text{-}SPh)_6(SPh)_4]$, and $(Me_4N)_4[Zn_{10}(\mu_3\text{-}S)_4(\mu_2\text{-}SPh)_{12}(SPh)_4]$ were prepared according to reported procedures.[3,6] The neutral $Zn_{10}(\mu_3\text{-}S)_4(\mu_2\text{-}SPh)_{12}$ was obtained by thermal decomposition of $(Me_4N)_4[Zn_{10}(\mu_3\text{-}S)_4(\mu_2\text{-}SPh)_{12}(SPh)_4]$.[6]

GC/MS spectra of volatile products obtained in the thermal decomposition of $(Me_4N)_4[Zn_{10}(\mu_3\text{-}S)_4(\mu_2\text{-}SPh)_{12}(SPh)_4]$ were obtained on a FISONS MD 800 instrument equipped with a 30 m (∅ = 0.25 mm) capillary column, using He as carrier gas and EI ionization. Elemental analyses were provided by the Microanalysis Laboratory of the Inorganic Chemistry Department of the University of Padova.

2.1.1. Synthesis of $(Me_4N)_2[Zn(SPh)_4]$.[3] To a solution of thiophenol (11.4 g, 103.5 mmol), Et_3N (10.45 g, 103.5 mmol), and Me_4NCl (3.75 g, 34 mmol) in 40 mL of MeOH was added 4.5 g (15 mmol) of $ZnNO_3\cdot 6H_2O$ in 20 mL of MeOH with stirring. The resulting solution was rapidly concentrated under vacuum until a solid began to form and then allowed to crystallize at −20 °C. The microcrystalline white solid was filtered off, washed with cold MeOH, and dried under vacuum.

$C_{32}H_{44}N_2S_4Zn$: yield 3.5 g, 5.4 mmol, 41%; mp = 186−187 °C. Elemental anal. Calcd: C, 59.10; H, 6.82; N, 4.31; S, 19.72. Found: C, 58.46; H, 6.71; N, 4.19; S, 19.34.

2.1.2. Synthesis of $(Me_4N)_2[Zn_4(\mu_2\text{-}SPh)_6(SPh)_4]$.[3] To a solution of thiophenol (10 g, 91 mmol) and Et_3N (9.25 g, 91 mmol) in 20 mL of MeOH was added 10.5 g (35.3 mmol) of $ZnNO_3\cdot 6H_2O$ in 35 mL of MeOH with vigorous stirring. Then 4.4 g (40 mmol) of Me_4NCl in 20 mL of MeOH was added to the mixture, and the resulting solution was concentrated under vacuum. By standing at −20 °C for 12 h, it yielded a viscous oil that changed into a white solid by prolonged sonification (20 min). This was then filtered off, washed with cold MeOH, and dried under vacuum.

$C_{68}H_{74}N_2S_{10}Zn_4$: yield 10.8 g, 7.2 mmol, 81.5%; mp = 198−199 °C. Elemental anal. Calcd: C, 54.40; H, 4.97; N, 1.87; S, 21.35. Found: C, 54.58; H, 4.86; N, 1.87; S, 21.18.

2.1.3. Synthesis of $(Me_4N)_4[Zn_{10}(\mu_3\text{-}S)_4(\mu_2\text{-}SPh)_{12}(SPh)_4]$.[3] To a solution of $(Me_4N)_2[Zn_4(\mu_2\text{-}SPh)_6(SPh)_4]$ (10 g, 6.6 mmol) in 150 mL of CH_3CN was added 106 mg (3.3 mmol) of sulfur (powder). The suspension was vigorously stirred at RT until a clean, light-yellow solution was obtained. By standing at RT for 48 h white crystals were formed. They were filtered off, washed with cold CH_3CN, and dried under vacuum. Additional crystals (80 mg) were obtained on cooling the mother liquors.

$C_{112}H_{128}N_4S_{20}Zn_{10}$: yield 1.5 g, 0.53 mmol, 20%. Elemental anal. Calcd: C, 47.61; H, 4.57; N, 1.98; S, 22.70. Found: C, 47.39; H, 4.35; N, 1.89; S, 23.08.

2.1.4. Synthesis of $Zn_{10}(\mu_3\text{-}S)_4(\mu_2\text{-}SPh)_{12}$.[6] $(Me_4N)_4[Zn_{10}(\mu_3\text{-}S)_4(\mu_2\text{-}SPh)_{12}(SPh)_4]$ (0.54 g, 0.19 mmol) was heated under vacuum (0.1 mmHg) at 240 °C for 6 h. During this time all volatiles were collected, and their GC/MS spectra revealed the presence of Me_3N (*m/z* 58) and PhSMe (*m/z* 124). The white solid residue was collected, washed with *n*-hexane, and dried under vacuum.

$C_{72}H_{60}S_{16}Zn_{10}$: yield 0.38 g, 0.18 mmol, 95%. Elemental anal. Calcd: C, 41.34; H, 2.89; S, 24.52. Found: C, 41.55; H, 2.86; S, 25.18.

2.2. Absorption Spectra. RT absorption spectra of PhSH and thiophenolate-capped clusters were recorded in the 200−500 nm region using a Varian Cary 5E spectrophotometer with a spectral band width of 1 nm; 10^{-5}−10^{-6} M solutions, obtained by dissolving the compounds in spectral grade CH_3CN (Aldrich), were employed immediately after their preparation.

2.3. X-ray Photoelectron Spectroscopy. A Perkin-Elmer PHI 5600ci spectrometer with monochromatized Al Kα radiation (1486.6 eV) was used for the XPS analyses. The working pressure was less than 2×10^{-7} Pa. The spectrometer was calibrated by assuming the binding energy (BE) of the Au $4f_{7/2}$ line at 83.9 eV with respect to the Fermi level. As an internal reference for the peak positions the C1s

peak of hydrocarbon contamination has been assumed at 284.8 eV.[20] Survey scans (187.85 eV pass energy; 1 eV step; 0.5 s/step dwell time) were obtained in the BE range between 0 and 1350 eV. Detailed scans were recorded at 5.85 eV pass energy, 0.1 eV step; 1.0 s/step dwell time for the Zn ($2p_{3/2}$ and $2p_{1/2}$), S ($2p_{3/2+1/2}$), N 1s, and C 1s lines, together with the corresponding valence band spectra.

The standard deviation in the BE values of the XPS lines is 0.10 eV. After a Shirley-type background subtraction,[21] the raw spectra were fitted using a nonlinear least-squares fitting program adopting Gaussian−Lorentzian peak shapes for all of the peaks.[22] The atomic compositions were evaluated using sensitivity factors as determined from theoretical photoionization cross sections and asymmetry parameters calculated within the Hartree−Fock−Slater one-electron central potential model.[23] The assignment of XPS peaks was carried out by referring to the handbook of X-ray PE spectroscopy[24] and to the X-ray PE spectroscopy database.[25]

2.4. Molecular Cluster Calculations. All of the calculations have been run by using the DMOL software package,[26] which allows the *ab initio* numerical solution of the Kohn−Sham equations for finite systems, providing energy eigenvalues, eigenvectors, and charge distribution and allowing the analytic evaluation of energy gradients (force calculations) by using numeric atomic orbital (NAO) basis sets.

We had already found[27] the adequacy of double numerical basis sets, obtained by augmenting the functions of the neutral atoms by the atomic valence functions of the corresponding 2+ ions (bond lengths and bond angles are usually converged within ∼0.01 Å and 1°, respectively). The following NAOs have been employed: (a) for Zn, the 1s−4s NAOs of the neutral zinc atom and the 3d−4p NAOs of Zn^{2+}; (b) for S, the 1s−3p NAOs of the neutral sulfur atom and the 3s−3d NAOs of S^{2+}. Two distinct extended basis sets have been used for C and H atoms: (c) for C, the 1s−2p NAOs of the neutral carbon atom and the 2s−2p NAOs of C^{2+} for C atoms belonging to Ph ligands; (d) the 1s−2p NAOs of the neutral carbon atom, the 2s−2p NAOs of C^{2+} and two sets of 1s, 2p, and 3d NAOs generated from two hydrogenic calculations using $Z = 5$ and $Z = 7$ for C atoms belonging to the Ph ring of the PhSH and PhS^- molecular/ionic free species; (e) the 1s NAO of the neutral hydrogen atom and the 1s NAO generated from a hydrogenic calculation using $Z = 1.3$ for H atoms belonging to Ph ligands; (f) the 1s NAO of the neutral hydrogen atom and two sets of 1s and 2p NAOs generated from two hydrogenic calculations using $Z = 1.3$ and $Z = 4$ for H atoms used in place of the Ph groups (see next section) or belonging to the Ph ring of the PhSH and PhS^- molecular/ionic free species. The Zn 1s−2p and the S, C 1s NAOs have been kept frozen in a fully occupied configuration allowing their exclusion from the variational space. Detailed information about the numerical integration scheme is reported in ref 26a; here it is sufficient to specify that ≤1000 sample points/atom have been used. As far as the *l* value of the one-center expansion of the coulomb potential about each nucleus is concerned, a value of *l* that is 1 greater than that in the atomic basis set has been found to provide sufficient precision.[26a] Here we adopted, for the whole series investigated, the following degree of angular truncation: $l = 3$ for Zn, and $l = 2$ for S, C, and H.

A well-known drawback of the local density approximation (LDA)[28] is the overestimation of the atomization energies. Such a deceit can be partially overcome by using gradient-corrected exchange−correlation functionals.[29] In our case we are not interested in total energy values; thus, because of the very large size of some of the clusters investigated, all of the numerical experiments have been carried out by adopting the LDA.

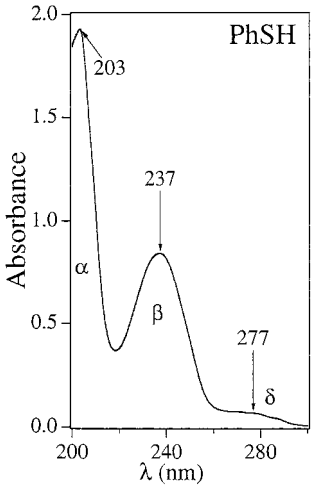

Figure 2. UV spectra of PhSH in CH_3CN.

As in previous contributions,[27,30] information about electronic states over a broad range of energies is provided by total and partial density of states (DOS and PDOS, respectively) diagrams,

$$\mathrm{PDOS}^{\nu}_{nl}(\epsilon) = \sum_p f'_{nl,p} \frac{\gamma/\pi}{(\epsilon - \epsilon_p)^2 + \gamma^2} \quad (1)$$

$$\mathrm{DOS}(\epsilon) = \sum_{\nu,n,l} \mathrm{PDOS}^{\nu}_{nl}(\epsilon) = \sum_p \frac{g_p \gamma/\pi}{(\epsilon - \epsilon_p)^2 + \gamma^2} \quad (2)$$

where $f'_{nl,p}$ is the Mulliken population[31] contribution from atom ν, state (nl), to the pth molecular orbital (MO) of energy ϵ_p and degeneracy g_p. The Lorentzian broadening factor γ has been set equal to 0.3 eV. All of the calculations have been performed on an IBM 6000/550 workstation at the C.I.M.A. department of the University of Padova.

3. Results and Discussion

3.1. Absorption Spectroscopy Measurements. The electronic absorption spectrum of PhSH in CH_3CN between 350 and 200 nm is reported in Figure 2 (wavelengths of the spectral features and molar absorptivities are reported in Table 1).[32] It consists of three bands labeled α, β, and δ lying at energies very close to those reported by Schweig *et al.*[34] for PhSH in heptane (204, 236, and 280 nm, respectively). The spectra of the ionic/neutral clusters measured immediately after dissolution in CH_3CN are shown in Figure 3. The comparison with data pertaining to PhSH and PhS^- [33] indicates that the spectral region extending from 200 to 300 nm is dominated by transitions mainly localized on the μ_2-bridging and terminal thiophenolates. Furthermore, inspection of Table 1 shows that the absorption bands are very strong, indicating that the relative transitions

(20) Seah, M. P.; Smith, G. C. In *Practical Surface Analysis*, 2nd ed.; Briggs, D., Seah, M. P., Eds.; Wiley: Chichester, 1990; Vol. 1, Appendix 1, pp 543−544.
(21) Shirley, D. A. *Phys. Rev.* **1972**, *55*, 4709.
(22) Vegh, J. *J. Electron Spectrosc. Relat. Phenom.* **1988**, *46*, 411.
(23) Yeh, J. J.; Lindau, I. Atomic Subshell Photoionization Cross Section and Asymmetry Parameteres: $1 \le Z \le 103$. *At. Data Nucl. Data Tables* **1985**, *32*, 1.
(24) Moulder, J. F.; Stickle, W. F.; Sobol, P. E.; Bomben, K. D. In *Handbook of X-ray Photoelectron Spectroscopy*; Chastain, J.; Ed.; Perkin Elmer Corp.: Eden Prairie, MN, 1992.
(25) *X-ray Photoelectron Spectroscopy Database*, version 1.0; National Institute of Standards and Technology: Gaithersburg, MD, 1989.
(26) (a) Delley, B. *J. Chem. Phys.* **1990**, *92*, 508. (b) Delley, B. *J. Chem. Phys.* **1991**, *94*, 7245.
(27) (a) Casarin, M.; Tondello, E.; Vittadini, A. *Surf. Sci.* **1994**, *303*, 125 and references therein. (b) Casarin, M.; Tondello, E.; Vittadini, A. *Surf. Sci.* **1994**, *307−309*, 1182. (c) Casarin, M.; Tondello, E.; Vittadini, A. *Inorg. Chim. Acta* **1995**, *235*, 151.
(28) Ziegler, T. *Chem. Rev.* **1991**, *91*, 651.
(29) Burke, K.; Perdew, J. P.; Levy, M. in *Modern Density Functional Theory: A Tool for Chemists*; Seminario, J. M., Politzer, P., Eds.; Elsevier Science B.V.: Amsterdam, 1995.
(30) (a) Casarin, M.; Maccato, C.; Tondello, E.; Vittadini, A. *Surf. Sci.* **1995**, *343*, 115. (b) Casarin, M.; Maccato, C.; Tabacchi, G.; Vittadini, A. *Surf. Sci.* **1996**, *352−354*, 341.
(31) Mulliken, R. S. *J. Chem. Phys.* **1955**, *23*, 1833.
(32) The electronic absorption spectrum of the PhS^- in CH_3CN is discussed in ref 33.
(33) Turk, T.; Resch, U.; Fox, M. A.; Vogler, A. *J. Chem. Phys.* **1992**, *96*, 3818.
(34) Schweig, A.; Diehl, F.; Kesper, K.; Meyer, H. *J. Mol. Struct.* **1989**, *198*, 307.

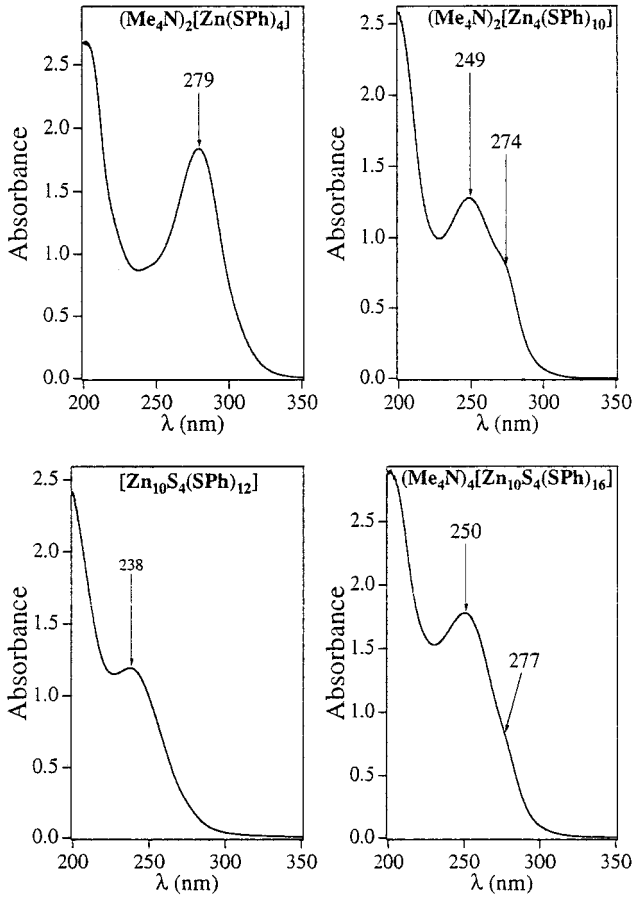

Figure 3. UV spectra of $[Zn(SPh)_4]^{2-}$ (**1**), $[Zn_4(\mu_2\text{-}SPh)_6(SPh)_4]^{2-}$ (**2**), $Zn_{10}(\mu_3\text{-}S)_4(\mu_2\text{-}SPh)_{12}$ (**3**), and $[Zn_{10}(\mu_3\text{-}S)_4(\mu_2\text{-}SPh)_{12}(SPh)_4]^{4-}$ (**4**) in CH_3CN.

Table 1. Wavelengths (nm) and Molar Absorptivities (in Parentheses in $l \times mol^{-1} \times cm^{-1}$) of C_6H_5SH, $(Me_4N)_2[Zn(SPh)_4]$, $(Me_4N)_2[Zn_4(\mu_2\text{-}SPh)_6(SPh)_4]$, $Zn_{10}(\mu_3\text{-}S)_4(\mu_2\text{-}SPh)_{12}$, and $(Me_4N)_4[Zn_{10}(\mu_3\text{-}S)_4(\mu_2\text{-}SPh)_{12}(SPh)_4]$ Absorption Spectra

species	UV bands
C_6H_5SH	203 (251 708)
	237 (110 042)
	277 (8906)
$(Me_4N)_2[Zn(SPh)_4]$	279 (49 400)
$(Me_4N)_2[Zn_4(\mu_2\text{-}SPh)_6(SPh)_4]$	249 (96 240)
	274 (61 128)
$Zn_{10}(\mu_3\text{-}S)_4(\mu_2\text{-}SPh)_{12}$	238 (113 524)
$(Me_4N)_4[Zn_{10}(\mu_3\text{-}S)_4(\mu_2\text{-}SPh)_{12}(SPh)_4]$	250 (167 453)
	277 (78 019)

are fully allowed. Two characteristic features are present in the spectra: (i) a band/shoulder at $\lambda > 270$ nm in the ionic clusters **1**, **2**, and **4** and (ii) an intense band peaking near/below 200 nm in the whole series. Even though Turk *et al.*[33] assigned the bands above 220 nm of the Cd analogues of **1**, **2**, and **4** (hereafter $\mathbf{1}_{Cd}$, $\mathbf{2}_{Cd}$, and $\mathbf{4}_{Cd}$) in CH_3CN to ligand-to-metal charge transfer (LMCT) transitions, the results reported by Liu *et al.*[16] allow us to foresee that both absorptions are mainly due to intraligand excitations. Differences between the spectra of Zn and Cd ionic derivatives simply regard the resolution of the feature at $\lambda > 270$ nm which, even if well evident, is a shoulder in **2** and **4** rather than a band as in $\mathbf{2}_{Cd}$ and $\mathbf{4}_{Cd}$.[33] Finally, the UV spectra of **3** and $Zn_{10}(\mu_3\text{-}S)_4(\mu_2\text{-}SEt)_{12}$[5] in CH_3CN are significantly different.

3.2. XPS Measurements. The XP valence band spectra of $(Me_4N)_2[Zn(SPh)_4]$, $(Me_4N)_2[Zn_4(\mu_2\text{-}SPh)_6(SPh)_4]$, $Zn_{10}(\mu_3\text{-}S)_4(\mu_2\text{-}SPh)_{12}$, and $(Me_4N)_4[Zn_{10}(\mu_3\text{-}S)_4(\mu_2\text{-}SPh)_{12}(SPh)_4]$ are reported in Figure 4. All of the spectra show three bands

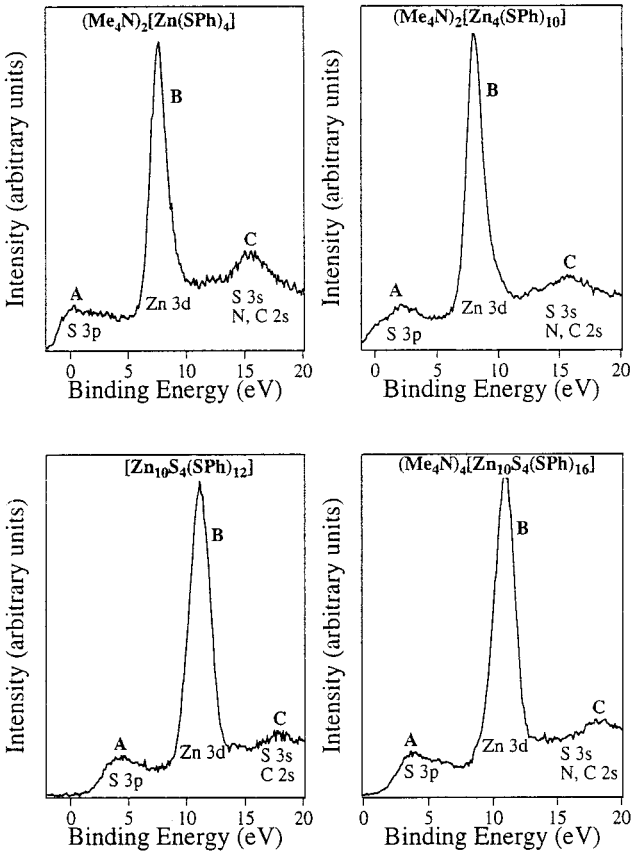

Figure 4. XPS valence band (Al Kα) of $(Me_4N)_2[Zn(SPh)_4]$, $(Me_4N)_2[Zn_4(\mu_2\text{-}SPh)_6(SPh)_4]$, $Zn_{10}(\mu_3\text{-}S)_4(\mu_2\text{-}SPh)_{12}$, and $(Me_4N)_4[Zn_{10}(\mu_3\text{-}S)_4(\mu_2\text{-}SPh)_{12}(SPh)_4]$.

alphabetically labeled. Reference to atomic subshell photoionization cross sections[23] indicates that detectable contributions derive from Zn 3d and S 3p−3s AOs ($\sigma_{Zn_{3d}} = 0.12 \times 10^{-1}$ Mb; $\sigma_{S_{3p}} = 0.10 \times 10^{-2}$ Mb; $\sigma_{S_{3s}} = 0.19 \times 10^{-2}$ Mb) as well as from N and C 2s levels ($\sigma_{N_{2s}} = 0.11 \times 10^{-2}$ Mb; $\sigma_{C_{2s}} = 0.66 \times 10^{-3}$ Mb), while contributions from N and C 2p AOs and the H 1s AO are negligible ($\sigma_{N_{2p}} = 0.72 \times 10^{-4}$ Mb; $\sigma_{C_{2p}} = 0.10 \times 10^{-4}$ Mb; $\sigma_H = 0.20 \times 10^{-5}$ Mb). Furthermore, referring to atomic ionization energies (IEs), we expect that bands **A**, **B**, and **C** will be largely due to ionizations from MOs mainly localized on S 3p, Zn 3d, and S (N, C) 3s (2s) AOs, respectively.

3.3. Theoretical Results. As already mentioned, both Gurin[14] and Han *et al.*[15] drastically solved the problem of the presence of phenyl groups bonded to terminal and μ_2-bridging S atoms by running their calculations on highly charged naked clusters of T_d symmetry. Han *et al.*[15] performed a series of discrete variational Xα calculations to investigate ground and excited states of the bare molecular ions $M_{10}E_4^{12+}$ (M = Cd, Zn; E = S, Se), i.e., the core of $(Me_4N)_4[M_{10}(\mu_3\text{-}E)_4(\mu_2\text{-}SPh)_{12}(SPh)_4]$. They adopted an adamantane-like cluster containing a tetrahedrally disposed set of four μ_4-E atoms, an octahedron of six bridging metal atoms, and an outer tetrahedron of four terminal metals. In this regard, it is worthwhile to point out that (i) the four E species present in $(Me_4N)_4[M_{10}(\mu_3\text{-}E)_4(\mu_2\text{-}SPh)_{12}(SPh)_4]$ occupy C_{3v} coordinatively unsaturated tetrahedral positions with a pyramidal (μ_3) arrangement (see Figure 1); (ii) no tetrahedral μ_4-E species is present in $(Me_4N)_4[M_{10}(\mu_3\text{-}E)_4(\mu_2\text{-}SPh)_{12}(SPh)_4]$;[3] (iii) the smallest cluster so far synthesized with a μ_4-E atom coordinated to four M ions is $Zn_4(\mu_4\text{-}S)\{\mu_2\text{-}$

$S_2As(CH_3)_2\}_6$;[35] and (iv) the presence of a sharp excitonic feature at 351 nm (3.53 eV)[9] in the absorption spectrum of $[Cd_{20}(\mu_4\text{-}S)(\mu_3\text{-}S)_{12}(\mu_2\text{-}SPh)_{18}(SPh)_4]^{8-}$ was ascribed to the presence of a $(\mu_4\text{-}S)Cd_4$ inner core. For these reasons, we are convinced that theoretical data reported in ref 15 have to be taken into account with some care.

A first-principle investigation of **4** is beyond the capability of our computational resources. Consequently, calculations on the real clusters were carried out only for **1**−**3**, while the whole series has been studied by considering simpler model compounds where the Ph groups were replaced by H atoms ($[Zn(SH)_4]^{2-}$ (**1***), $Zn_4[(\mu_2\text{-}SH)_6(SH)_4]^{2-}$ (**2***), $Zn_{10}(\mu_3\text{-}S)_4(\mu_2\text{-}SH)_{12}$ (**3***), and $[Zn_{10}(\mu_3\text{-}S)_4(\mu_2\text{-}SH)_{12}(SH)_4]^{4-}$ (**4***)). Insights into the perturbations induced by replacing the Ph ligands with H atoms on terminal and μ_2-bridging S have been obtained by comparing the electronic properties of PhS^- and HS^- ions (see next section).

3.3.1. Thiophenole and Thiophenolate. Calculations for the protonated (deprotonated) species have been carried out in a C_s (C_{2v}) symmetry and by adopting basis sets b, d, and f. The valence manifold of PhSH is characterized by five frontier π orbitals, three of them (π^{b}_{Ph-S}, π_{Ph}, and π^{ab}_{Ph-S})[36] occupied and two empty (π^{*}_{Ph}). Interestingly, despite the low symmetry of the neutral molecule (C_S), the degeneracy of the π^{*}_{Ph} MOs is only slightly affected as a consequence of the negligible involvement of the S $3p_\pi$ AO. The following excitations between occupied and empty π orbitals have been computed through spin polarized transition state (TS) calculations:[37] $\pi^{ab}_{Ph-S} \rightarrow \pi^{*}_{Ph}$ 286 nm; $\pi_{Ph} \rightarrow \pi^{*}_{Ph}$ 234 nm; and $\pi^{b}_{Ph-S} \rightarrow \pi^{*}_{Ph}$ 196 nm. The agreement between theory and experiment is very good (see Figure 2 and Table 1) and not limited to electronic transitions.[38]

Turning now to examine the PhS^- outermost occupied MOs, we find a new level close in energy to the π^{ab}_{Ph-S} MO ($4b_2$): the in-plane S lone pair (n_S-7b_1 MO) previously involved in the S−H bonding. Furthermore, the π^{*}_{Ph} level degeneracy (see above) is lifted as a consequence of the significant involvement of the S $3p_\pi$ AO in one of them ($5b_2$ MO). Spin polarized TS calculations[37] for electronic excitations from the outermost occupied orbitals to the empty $2a_2$ and $5b_2$ π^{*}_{Ph} levels give the following results: $\pi^{ab}_{Ph-S} \rightarrow \pi^{*}_{Ph}$, 387 ($2a_2$), 391 ($5b_2$) nm; $n_S \rightarrow \pi^{*}_{Ph}$ ($2a_2$), 322 nm;[40] $\pi_{Ph} \rightarrow \pi^{*}_{Ph}$, 238 ($2a_2$), 222 ($5b_2$) nm; and $\pi^{b}_{Ph-S} \rightarrow \pi^{*}_{Ph}$, 216 ($2a_2$), 201 ($5b_2$) nm. It must be remarked also that the energy of the band at 303 nm in the UV spectrum of PhS^- [33] is poorly reproduced.

It is now important to summarize the main effects due the replacement of the Ph rings with H atoms, i.e., on passing from PhS^- to HS^-. We find that the S 3p pairs are destabilized[41] and the S gross atomic charge (Q_S) is increased (from −0.75 to −0.85), indicating that the Ph fragment acts as an electron reservoir.[42] Such results shall be useful in the forthcoming discussion regarding the electronic structure of the clusters.

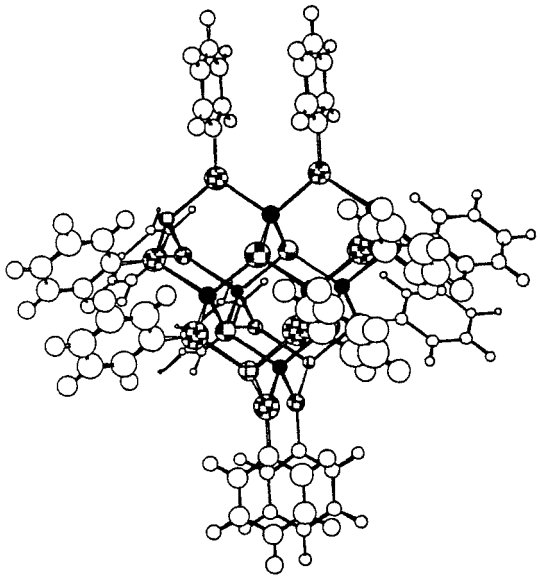

Figure 5. Ball and stick representation of the idealized $Zn_{10}(\mu_3\text{-}S)_4(\mu_2\text{-}SPh)_{12}$ (**3**).

3.3.2. $[Zn(SPh)_4]^{2-}$ and $[Zn_4(\mu_2\text{-}SPh)_6(SPh)_4]^{2-}$. A quantitative estimate of the energy shift induced on the S 3p pairs by the H replacement of the Ph rings has been obtained by carrying out a series of ground state calculations on **1**, **1***, **2**, and **2***. Their geometry has been fully optimized in a D_{2d} symmetry, even though it is known that **2** possesses neither crystallographic symmetry nor any approximate symmetry.[43,44] On the other hand, it is also known[44] that systems such as $[M_{4-n}M'_n(\mu_2\text{-}SPh)_6(SPh)_4]^{2-}$ (M, M′ = Fe(II), Co(II), Zn(II), Cd(II)), having an adamantane-like structure, are characterized at RT by a stereochemical nonrigidity of the $[M_4(\mu_2\text{-}SPh)_6(SPh)_4]^{2-}$ cages, which results in equilibration of bridging and terminal ligands. A further numerical experiment, limited to molecular orbital analysis, has been carried out for $Zn_{10}(\mu_3\text{-}S)_4(\mu_2\text{-}SPh)_{12}$, idealizing its structure to a T_d symmetry (see Figure 5).[45]

Geometrical parameters of **1**, **1***, **2,** and **2***, collected in Table 2, agree with available crystallographic data.[46,47] Information about the electronic structure of **1** and **2** is provided by Figure 6, where the DOS of **1**, **1***, **2**, and **2*** are displayed. The analysis of theoretical data pertaining to **1** and **1*** indicates that (i) the HOMO energy of **1** (0.97 eV) is ∼1.7 eV lower than that of **1*** (2.70 eV);[48] (ii) the outermost occupied MOs of **1** and **1*** are mainly composed of the S 3p pairs; and (iii) at variance to **1***,

(35) Johnstone, D.; Fergusson, J. E.; Robinson, W. T. *Bull. Chem. Soc. Jpn.* **1972**, *45*, 3721.

(36) π^{b}_{Ph-S} and π^{ab}_{Ph-S} stand for bonding and antibonding combinations between one of the Ph e_{1g} π orbitals and the S $3p_\pi$ AO; π_{Ph} is the second partner of the Ph-based e_{1g} π MOs, nonbonding with respect to the interaction with S. In the adopted framework, the π character corresponds to the *Z* direction.

(37) Slater, J. C. *Quantum Theory of Molecules and Solids. The Self-Consistent Field For Molecules and Solids*; McGraw-Hill: New York, 1974; Vol. 4.

(38) The IE region below 11 eV of the He I spectrum of PhSH shows the presence of three well-resolved bands with IEs 8.28, 9.38 and 10.65 eV, assigned by Frost *et al.*[39] to the ionization from the π^{ab}_{Ph-S}, π_{Ph}, and π^{b}_{Ph-S} MOs. Theoretical IEs, evaluated through spin-polarized TS calculations,[37] are 8.47, 9.80, and 10.54 eV, respectively.

(39) Frost, D.; Herring, F.; Katrib, A.; McDowell, C.; McLean, R. *J. Phys. Chem.* **1972**, *76*, 1030.

(40) Within the assumed symmetry (C_{2v}), the n_S ($7b_1$) → π^{*}_{Ph} ($5b_2$) transition is forbidden by electric dipole selection rules.

(41) In HS^- the S 3p pairs are degenerate at 1.25 eV. In the C_{2v} symmetry such a degeneration is lifted and 3p pairs, transforming as b_1 and b_2, lie at 0.12 and 0.17 eV, respectively.

(42) Calculations on PhSH and PhS^- carried out with basis sets b, c, and e give exactly the same results. Minor differences are limited to total energy values.

(43) Hencher, J. L.; Khan, M.; Said, F. F.; Tuck, D. G. *Inorg. Nucl. Chem. Lett.* **1981**, *20*, 2155.

(44) Hagen, K. S.; Stephan, D. W.; Holm, R. H. *Inorg. Chem.* **1982**, *21*, 3928.

(45) The Zn−S and S−Ph bond lengths are set at 2.36 and 1.78 Å, respectively.

(46) Swenson, D.; Baenziger, N. C.; Coucouvanis D. *J. Am. Chem. Soc.* **1978**, *100*, 1935.

(47) To our knowledge, the only structural determination of a zincmantane derivative is reported in ref 43, where no information about the Ph fragments is included. In Table 2 we referred to the X-ray diffraction data obtained for the isostructural ferromantane[44] to get some hints of the Ph geometry.

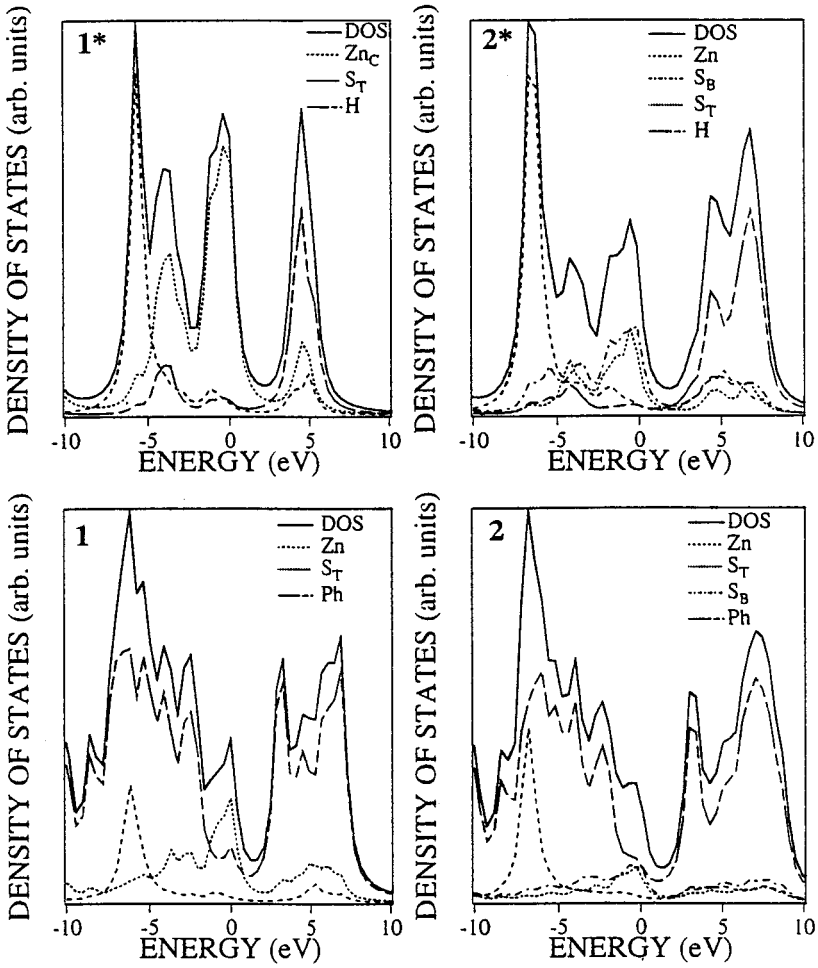

Figure 6. Density of states of $Zn(SH)_4^{2-}$ (**1***), $[Zn_4(\mu_2\text{-}SH)_6(SH)_4]^{2-}$ (**2***), $Zn(SPh)_4^{2-}$ (**1**), and $[Zn_4(\mu_2\text{-}SPh)_6(SPh)_4]^{2-}$ (**2**). Plots of partial density of states of Zn, S_B, S_T, Ph, and H are also displayed. For each cluster the energy scale origin corresponds to the E_{HOMO}.

Table 2. Optimized Geometrical Parameters for $[Zn(SPh)_4]^{2-}$ (**1**), $[Zn(SH)_4]^{2-}$ (**1***), $[Zn_4(\mu_2\text{-}SPh)_6(SPh)_4]^{2-}$ (**2**), and $[Zn_4(\mu_2\text{-}SH)_6(SH)_4]^{2-}$ (**2***)[a]

	$Zn(SPh)_4^{2-}$	$Zn(SH)_4^{2-}$	$Zn_4(SPh)_{10}^{2-}$	$Zn_4(SH)_{10}^{2-}$
$Zn-S_T$	2.35 (2.35)[b]	2.36	2.31 (2.29)[c]	2.24
$Zn-S_B$			2.38 (2.37)[c]	2.34[e]
S_T-C_α	1.75		1.76 (1.78)[d]	
S_T-H		1.36		1.35
S_B-C_α			1.76	
S_B-H				1.35
$C-C^a$	1.40		1.39 (1.38)[d]	
$C-H^a$	1.09		1.10	
S_T-Zn-S_T	109 (110.4)	110		
$Zn-S_T-C_\alpha$	107		129	
$Zn-S_T-H$		90		91
$Zn-S_B-H$				118

[a] Bond lengths and bond angles in Å and deg, respectively. Experimental values are in parentheses. The symmetry assumed for **2** is D_{2d} (see text). This implies that the planes of the Ph groups bonded to the μ_2-S atoms positioned along the C_2 axis are forced to be either parallel or perpendicular to the same plane of the $Zn-\mu_2\text{-}S-Zn$ fragment. [b] Mean value from ref 46. [c] Mean value from ref 43. [d] Mean value from ref 44. [e] Mean value.

where S 3p pairs are grouped together, in **1** a component is hidden under the peak due to the π combinations deriving from the e_{1g} Ph MOs. This MO, characterized by a strong (62%) participation of the S 3p AOs parallel to the Ph planes, is one of the main sources of bonding between the S 3p and Zn 4s AOs (the total Zn−S overlap population (OP) is 0.277e).

As far as the low-lying unoccupied orbitals of **1** are concerned, they are strongly localized on the Ph rings (see Figure 6). In particular, the lowermost peak at positive energies is due to the linear combinations of the e_{2u} Ph-based π^* MOs. It is of relevance to stress that, even though the nature of the outermost occupied MOs in **1** and **1*** is similar, the lowermost unoccupied levels are completely different in the two cases: in **1** they derive from the e_{2u} Ph-based π^* orbitals (see above) while in **1*** they account for the antibonding S−H interaction. Nevertheless, the ΔE between the outermost occupied orbitals and the virtual Zn 4s AO is the same in both cases (5.30 eV), indicating that, in **1**, the replacing of Ph fragments with H atoms has only minor effects on the ΔE between the S 3p pairs and virtual Zn based MOs.

As already pointed out, a common feature of the UV spectra of compounds containing terminal thiophenolates (i.e., **1**, **2**, and **4**) is a band (in **1**) or a shoulder (in **2** and **4**) in the range 274−279 nm (see Figure 3 and Table 1). Inspection of Figure 6 reveals that the lowest lying transitions should involve the excitation of an electron from S 3p based MOs to π^* Ph levels. Results pertaining to the electronic structure of the PhS^- lead us to assign the band at 279 nm of **1** to the $\pi^{ab}_{Ph-S} \rightarrow \pi^*_{Ph}$ intraligand transitions,[49] while the low-wavelength side of this band, also in agreement with data reported by Liu *et al.*,[16] should

(48) Absolute energy values cannot be obtained from inspection of the DOS where the energy is scaled with respect to the HOMO. The HOMO energies are positive for **1***, **2***, and **4*** as well as for **1**, all of them carrying a negative charge (−2, −2, −4, and −2, respectively). In a series of preliminary numerical experiments on **1***, we verified that the inclusion of a positive, spherically symmetric, external potential had the only effect of uniformly shifting all of the energy levels at lower (negative) values. For this reason, the herein reported data have been obtained without the inclusion of any external positive potential.

include LMCT and $\pi_{Ph} \rightarrow \pi^*_{Ph}$ intraligand excitations. Finally, the band peaking below 200 nm is assigned to the $\pi^b_{Ph-S} \rightarrow \pi^*_{Ph}$ PhS^- based transitions.

The electronic structure of the zincmantane cage of **2** can be better understood by assuming an idealized T_d symmetry. The inorganic framework of **2** is constituted by three types of atoms: one type of zinc (Zn_C) and two types of sulfur (S_T and S_B). As a whole the S atoms participate with 30 3p AOs: 12 localized on the *terminal* S (the T set) and 18 on the *bridging* μ_2-S (the B set). Set T consists of four σ orbitals (pointing toward the Zn atoms) and eight π orbitals. Under the T_d symmetry, T_σ spans the $a_1 + t_2$ irreducible representations while T_π spans the $e + t_1 + t_2$ ones. As far as the B set is concerned, it is composed of six lone pairs[50] ($a_1 + e + t_2$) directed toward the center of the cage (B_σ) and 12 nonbonding levels (B_π, $2t_1 + 2t_2$). The set B_π can be further broken down into two subsets, one purely nonbonding and perpendicular ($\perp$) to the $Zn-S_B-Zn$ plane ($t_1 + t_2$), the other ($t_1 + t_2$) parallel ($\parallel$) to the same plane and reasonably involved in the S_B-Zn σ interaction.

As already found in **1** and **1***, the HOMO of **2** lies deeper in energy (−0.81 eV) than that of **2*** (0.28 eV). Moreover, in agreement with the above reported qualitative scheme, the outermost 14 MOs of **2** ($a_1 + b_1 + 2a_2 + 2b_2 + 4e$ in the D_{2d} symmetry) are mostly based on T_π and the $B^\perp_\pi$ subset. As far as the remaining sixteen orbitals ($T_\sigma + B_\sigma + B^\parallel_\pi$) are concerned, they lie, strongly admixed, in the same energy region of Ph-based levels (see Figure 6). Further insights can be gained by comparing the Zn−S OPs and Q values of **1** and **2**. The $Zn-S_T$ OP is substantially the same on passing from **1** (0.277e) to **2** (0.271e) while a smaller value (0.206e) is computed for the $Zn-S_B$ OP. Such a decrease, due to the participation of each S_B in two bonds with Zn atoms, could be a reasonable explanation of the above mentioned zincmantane cage stereochemical nonrigidity. As far as the Q values are concerned, the following points should be stressed: (i) Q_{Zn} is very similar in **1** and **2** (0.46 and 0.47, respectively); (ii) Q_{ST} is definitely more negative in **1** than in **2** (−0.57 and −0.43, respectively); (iii) Q_{ST} and Q_{SB} (−0.44) are very close in **2**; (iv) the Ph charge is always very small −0.05 in **1**, −0.01 and 0.09 for Ph groups bonded to S_T and S_B in **2**, respectively). As a whole, these data indicate that (i) the electronic structure of the Zn atoms is only slightly influenced by the nature (terminal or bridging) of their ligands; (ii) most of the negative charge carried by the ions is localized on the most electronegative species (the S atoms);[51] and (iii) the electron reservoir role of the Ph group is confirmed.

Besides the increased energy level overcrowding of **2**, both below and above the zero energy, a further important difference between the DOS of **1** and **2** is found in the energy range covered by Zn virtual levels (see Figure 6). Actually, in **2** these contributions are smeared out over an energy interval larger than in **1**, preventing the possibility of associating LMCT excitations with a specific band. According to that, the absorption pattern of **2** is dominated by intraligand transitions, as found in $\mathbf{2}_{Cd}$.[16] Nevertheless, an experimental chromophore factoring is possible. We already pointed out that a common feature of UV spectra of **1**, **2**, and **4** (see section 3.1) is an absorption at $\lambda > 270$ nm. On this basis, we propose to assign the shoulder at 274 nm to $\pi^{ab}_{Ph-S} \rightarrow \pi^*_{Ph}$ excitations mainly localized on the terminal thiophenolates and the broad band at 249 nm to intraligand transitions involving both terminal and bridging ligands. As in **1**, the band peaking below 200 nm is ascribed to $\pi^b_{Ph-S} \rightarrow \pi^*_{Ph}$ excitations. Before moving to the analysis of XPS data we want to mention that theoretical results do not reproduce the experimentally observed chromophore factoring, possibly because of the assumed idealized geometry.

Our calculations are also in good agreement with XPS data of **1** and **2**. Actually, referring to the DOS of **1** and keeping in mind the discussion of section 3.2, we confidently assign the broad band **A** to the ionization from S_T 3p levels, band **B** to the Zn 3d atom-like orbitals, and finally, band **C** to the ionization from MOs mainly localized on S_T 3s and N, C 2s AOs. Both the energy spread of band **B** (∼1.7 eV) and the ΔE between the onset of band **A** and **B** (7.5 eV) are satisfactorily reproduced by theoretical calculations (∼1.6 and 6.1 eV, respectively).[52]

XPS data pertaining to **2** indicate that the full width at half maximum (FWHM) of band **B** (once more associated with the ionization from atom-like Zn 3d AOs) is the same (1.75 eV) as in **1**. Furthermore, taking **B** as a reference, band **A** lies at a higher IE in **2** than in **1**, while band **C** does not show any significant modifications moving from **1** to **2**. These evidences are indicative of a shift toward higher ionization energies of levels localized on S_T and S_B 3p AOs in **2**, in agreement with the larger Q_S values in **1** than in **2**.

3.3.3. $Zn_{10}(\mu_3\text{-}S)_4(\mu_2\text{-}SPh)_{12}$ and $[Zn_{10}(\mu_3\text{-}S)_4(\mu_2\text{-}SPh)_{12}(SPh)_4]^{4-}$. The most peculiar feature of **3** is the presence of an equal number of Zn and S atoms (Zn_P and S_P, respectively) which miss one ligand (see Figure 1). Actually, the incomplete capping of Zn_P should give rise to localized low-lying empty surface states which could act as electron acceptor/trap upon electron excitation.[16] Particularly interesting also is the presence of the μ_3-S species; actually, the pyramidal S atoms bind only Zn atoms and occupy C_{3v} unsaturated tetrahedral positions, and their electronic structure should be dominated by the presence of a lone pair pointing in the direction of the missing ligand. The set of four μ_3-S lone pairs (P_n) spans, in T_d symmetry, the representations $t_2 + a_1$, while the remaining eight μ_3-S 3p AOs, constituting the P_π set, transform as $t_2 + t_1 + e$. Both the stereochemistry and the electronic structure of **3** would then make this compound a reasonable molecular model of ZnS nonpolar surfaces. In this regard, we want to emphasize that in III−V, II−VI, and I−VII semiconductor surfaces, *dangling bonds* localized on the surface atoms belonging to the V (III), VI (II), or VII (I) group are filled (empty) and point toward the direction of the missing ligand.[54]

Inspection of Figures 7 and 8, where the DOS of **3** and **3***[55] are respectively displayed, makes it evident that, independently of the presence of Ph ligands on μ_2-S, (i) the HOMO is strongly localized on μ_3-S atoms (the t_2 component of the P_n set); (ii) the LUMO is highly concentrated on the peripheral Zn_P atoms (the t_2 linear combinations, quasi-degenerate with the a_1 one, of 4s AOs); and (iii) the PDOS of Zn_P is shifted toward lower energies with respect to the PDOS of the completely saturated Zn_C. This shift is not uniform, being smaller for the occupied 3d atom-like AOs (1.22 eV) than for the virtual 4s levels (3.27 eV). According to the presence of a lone pair on each μ_3-S,

(49) In the assignment of UV absorption spectra of **1**−**4** we limited ourselves to consider ground state ΔE rather than using Slater's TS formalism[37] because, even in the simplest case, the number of transitions to be computed was very high.

(50) In the idealized zincmantane cage the six μ_2-S are placed at the vertices of an octahedron.

(51) Sanderson, R. T. *J. Chem. Educ.* **1952**, *29*, 539; **1956**, *33*, 443.

(52) It is known[53] that LDA underbinds the 3d levels.

(53) Zakharov, O.; Rubio, A.; Blase, X.; Cohen, M. L.; Louie, S. G. *Phys. Rev. B* **1994**, *50*, 10780.

(54) (a) Mariano, A. N.; Hanneman, R. E. *J. Appl. Phys.* **1963**, *34*, 384 and references therein reported. (b) Casarin, M.; Favero, G.; Tondello, E.; Vittadini, A. *Surf. Sci.* **1994**, *317*, 422.

(55) The electronic structure of **3*** and **4*** has been computed by adopting an idealized T_d symmetry where the Zn−S and S−H bond lengths are set at 2.36 and 1.35 Å, respectively.

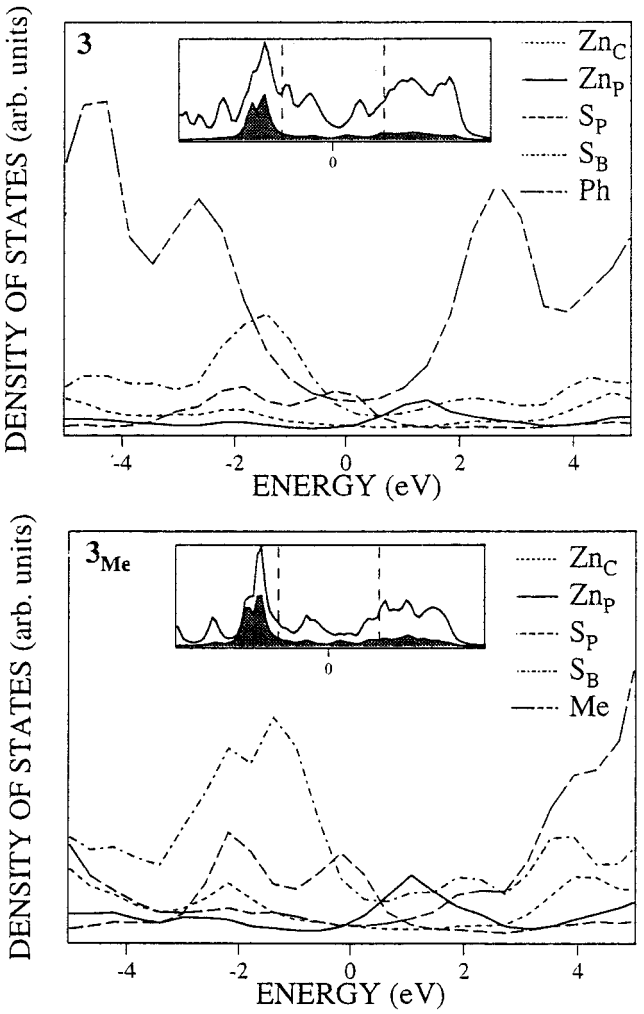

Figure 7. Density of states of $Zn_{10}(\mu_3\text{-}S)_4(\mu_2\text{-}SPh)_{12}$ (**3**) and $Zn_{10}(\mu_3\text{-}S)_4(\mu_2\text{-}SCH_3)_{12}$ ($\mathbf{3}_{Me}$). Plots of partial density of states of Zn_C, Zn_P, S_P, S_B, Ph and Me for **3** and $\mathbf{3}_{Me}$ in a narrower energy range are also reported. For both clusters the energy scale origin corresponds to the relative E_{HOMO}.

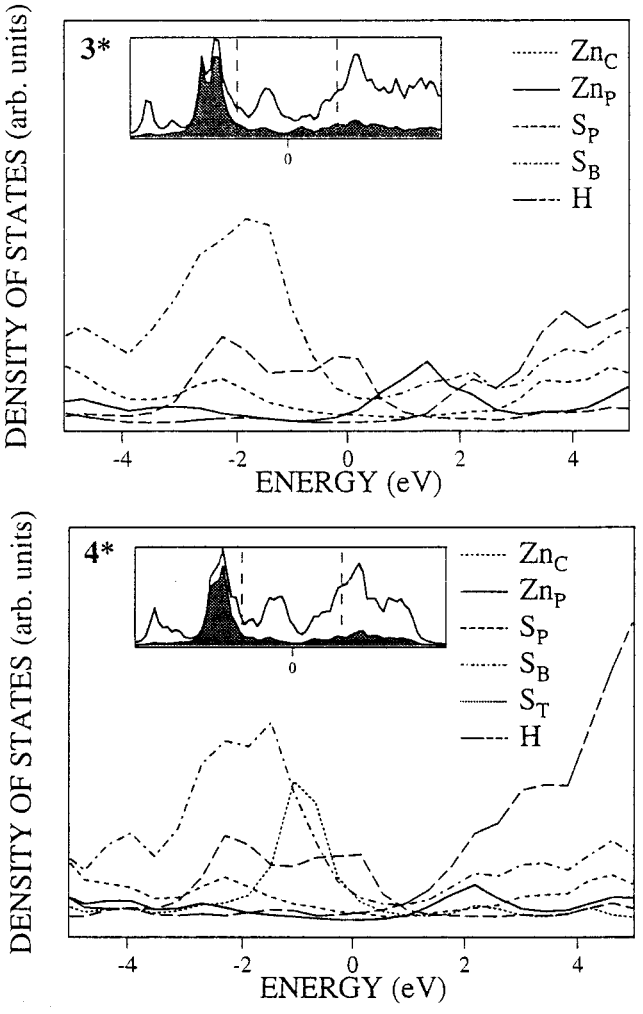

Figure 8. Density of states of $[Zn_{10}(\mu_3\text{-}S)_4(\mu_2\text{-}SH)_{12}(SH)_4]^{4-}$ (**4***) and $Zn_{10}(\mu_3\text{-}S)_4(\mu_2\text{-}SH)_{12}$ (**3***). Plots of partial density of states of Zn_C, Zn_P, S_P, S_B, and H for **4*** and **3*** in a narrower energy range are also reported. For both clusters the energy scale origin corresponds to the relative E_{HOMO}.

Q_{S_P} is significantly more negative (−0.63 and −0.61 in **3** and **3***, respectively) than Q_{S_B} (−0.45 and −0.48). Moreover, in agreement with results obtained for **2**, the weakest Zn−S interaction is computed between Zn_C and S_B atoms (the S_P−Zn_C, S_B−Zn_C, and S_B−Zn_P OPs are 0.245e, 0.189e, and 0.242e, respectively). This outcome is well in tune with the stereochemical nonrigidity of the zincmantane cage as well as with electron spray mass spectrometry results reported by Løver *et al.*[56] for $\mathbf{1}_{Cd}$, $\mathbf{2}_{Cd}$, and $\mathbf{4}_{Cd}$. Actually, the authors pointed out that (i) all of the investigated compounds show a great tendency to lose the PhS^- species; (ii) at a cone voltage of 20 V the most abundant fragment, besides PhS^-, is $[Cd(SPh)_3]^-$, which necessarily implies, in $\mathbf{2}_{Cd}$ and $\mathbf{4}_{Cd}$, the breaking of S_B−Cd_C bonds; and (iii) no fragmentation involving the S_P−Cd_C bonds in $\mathbf{4}_{Cd}$ is evidenced, indicating a high stability of the $(\mu_3\text{-}S)_4M_6$ inner core.[57]

Theoretical results (see Figure 7) indicate that the lowest electronic excitation is a LMCT transition between localized surface states (from the t_2 component of the P_n set to the a_1 + t_2 combinations of Zn_P 4s AOs). According to the calculations carried out by Liu *et al.*[16] on the hypothetical $[Cd_2(\mu_2\text{-}SPh)_2\text{-}SPh]^-$ and $[Cd_4(\mu_2\text{-}SPh)_6(SPh)_3]^-$ ions (models of a coordinative vacancy on a Cd atom), the presence of low-lying empty states would originate transitions with small oscillator strengths at the red end of the absorption spectrum.[58] Therefore, $Zn_{10}(\mu_3\text{-}S)_4\text{-}(\mu_2\text{-}SPh)_{12}$ fits both the stereochemical and electronic structure criteria to be a good molecular model[17] of nonpolar ZnS surfaces.

The UV absorption spectrum of **3** (see Figure 3) is characterized by an intense band peaking below 200 nm, attributed to $\pi^b_{Ph-S} \rightarrow \pi^*_{Ph}$ intraligand transitions, and a weaker band at 238 nm that we propose to assign as a whole to $\pi^{ab}_{Ph-S} \rightarrow \pi^*_{Ph}$, $\pi_{Ph} \rightarrow \pi^*_{Ph}$, and LMCT transitions from the t_2 component of the μ_3-S P_n set to the 4s AOs of Zn_C atoms.[60]

We already mentioned in section 3.1 that the absorption spectra in CH_3CN of **3** and $Zn_{10}(\mu_3\text{-}S)_4(\mu_2\text{-}SEt)_{12}$ are significantly different (the thioethanolate derivative exhibits a strong absorption at 280 nm and a weaker absorption at 320 nm).[5] A

(56) Løver, T.; Bowmaker, G. A.; Henderson, W.; Cooney, R. P. *Chem. Commun.* **1996**, 683.

(57) The smallest $(\mu_3\text{-}S)_4Cd_x$ fragment experimentally detected[56] is $(\mu_3\text{-}S)_4Cd_8$ in $[Cd_8(\mu_3\text{-}S)_4(SPh)_{10}]^{2-}$ deriving from the parent ion by loss of two $[Cd(SPh)_3]^-$ units.

(58) A recent DF study dealing with the surface band structure of the nonpolar ZnS(110) surface indicates that there are surface states in the fundamental gap arising from the empty cation-derived and the occupied anion-derived dangling bonds.[59]

(59) Ferraz, A. C.; Watari, K.; Alves, J. L. A. *Surf. Sci.* **1994**, *307*−*309*, 959.

(60) The absence of any terminal thiophenolate in **3** and the lack of any feature at $\lambda > 270$ nm reinforce the assignment we proposed for the UV spectra of **1** and **2**.

ground state calculation on the model $Zn_{10}(\mu_3\text{-}S)_4(\mu_2\text{-}SCH_3)_{12}$ ($\mathbf{3}_{Me}$) has been carried out to get an estimate of the role played by a σ-donor ligand on the electronic structure of the $Zn_{10}(\mu_3\text{-}S)_4(\mu_2\text{-}S)_{12}$ skeleton. Though the main features of the DOS/PDOS of $\mathbf{3}_{Me}$ and **3** are the same (see Figure 7), the ΔE between the HOMO and Zn_C 4s AOs is significantly smaller in the former (3.92 vs 4.69 eV). According to that, we propose to assign the weak band at 320 nm to LMCT transitions from the occupied μ_3-S P_n set to the empty Zn_C 4s AOs without invoking aggregation products of the cluster in solution, as suggested in ref 5. As far as the strong absorption band at 280 nm is concerned, it most probably includes transitions mainly localized on the μ_2-SR moieties. These data indicate that the significant blue shift in the UV spectrum of **3** compared to that of $\mathbf{3}_{Me}$ has to be ascribed to the different nature of the ligands, which seems to influence the energy of Zn_C 4s AOs much more than that of Zn_P. According to that, not only $Zn_{10}(\mu_3\text{-}S)_4(\mu_2\text{-}SPh)_{12}$ but, more generally, all of the $Zn_{10}(\mu_3\text{-}S)_4(\mu_2\text{-}SR)_{12}$ derivatives can be considered good molecular models of nonpolar ZnS surfaces.

Compound **4** differs from **3** for the presence of four terminal thiophenolates saturating the coordinative vacancy of peripheral Zn_P atoms (see Figure 1). The DOS of **4*** (see Figure 8) shows that the outermost occupied MOs are still localized on μ_3-S and, quite unexpectedly, the PDOS peaks of peripheral Zn atoms are still shifted toward lower energies, even though to a smaller extent than in **3**, with respect to that of the Zn_C atoms of the $(\mu_3\text{-}S)_4Zn_6$ core. The absorption spectrum of **4** (see Table 1 and Figure 3) consists of the strong absorption at ~200 nm, originated by $\pi^{b}_{Ph-S} \rightarrow \pi^{*}_{Ph}$ intraligand transitions, and of a band at 250 nm with a shoulder (277 nm) on its lower wavelength side. This last feature, according to previous assignments, is associated with $\pi^{ab}_{Ph-S} \rightarrow \pi^{*}_{Ph}$ intraligand excitations involving terminal thiophenolates, while the band at 250 nm should include the remaining intraligand and LMCT transitions implying the t_2 component of the μ_3-S P_n set and 4s AOs of the Zn atoms of the $(\mu_3\text{-}S)_4Zn_6$ core. At variance with UV spectral data pertaining to Cd analogues, negligible band shifts are found with cluster size increasing.[33]

Moving to XPS data, the assignment proposed for **1** and **2** still holds in **3** and **4** with bands **A** and **B** associated with the ionizations from MOs strongly localized on 3p S and 3d Zn AOs, respectively. As far as band **C** is concerned, it includes in **3** (**4**) contributions from the S 3s and C 2s AOs (S 3s and N, C 2s AOs). The FWHM of band **B** in **3** and **4** is larger than in **1** and **2**. Furthermore, it is wider in **3** (2.25 eV) than in **4** (2.00 eV) according to the presence, in the former, of two types of Zn atoms. On passing from **1**−**2** to **3**, theoretical data correctly reproduce variations of the Zn 3d band, while no difference is present in the theoretical FWHM of the Zn PDOS of **3*** and **4***.

3.3.4. $[Zn_{20}(\mu_4\text{-}S)(\mu_3\text{-}S)_{12}(\mu_2\text{-}SPh)_{18}(SPh)_4]^{8-}$. We already mentioned that the synthetic routes we successfully used for the synthesis of **1**−**4** were the same as those reported in the literature for the Cd analogues.[3,6] On this basis, the idea proposed by Herron *et al.*[9] to synthesize the ~10 Å thiophenolate cluster $[Cd_{20}(\mu_4\text{-}S)(\mu_3\text{-}S)_{12}(\mu_2\text{-}SPh)_{18}(SPh)_4]^{8-}$ by a careful addition of sulfide ions to a DMF solution of $\mathbf{4}_{Cd}$ has been here applied to obtain the analogous Zn derivative. Our interest for $[Zn_{20}(\mu_4\text{-}S)(\mu_3\text{-}S)_{12}(\mu_2\text{-}SPh)_{18}(SPh)_4]^{8-}$ (**5**) is due to its $(\mu_4\text{-}S)Zn_4(\mu_3\text{-}S)_{12}$ inner core, which in principle might be a molecular model of the solid ZnS.

The progressive addition of sulfide ions to a DMF solution of **4** has been carried out by simultaneously monitoring the UV absorption spectrum of the mixture. No sharp absorption was detected at $\lambda > 300$ nm when **4** and S^{2-} were mixed in the ratio 1:2.5, i.e., the ratio which according to eq 3 should be the right one to obtain **5**. The absence of any sharp feature might

$$2[Zn_{10}(\mu_3\text{-}S)_4(\mu_2\text{-}SPh)_{12}(SPh)_4]^{4-} + 5S^{2-} \rightarrow [Zn_{20}(\mu_4\text{-}S)(\mu_3\text{-}S)_{12}(\mu_2\text{-}SPh)_{18}(SPh)_4]^{8-} + 10SPh^{-} \quad (3)$$

be due either to the failure of the linking between the molecular precursors with the sulfide ions acting as cement or to a blue shift, in the Zn derivative, of the excitonic transition lying at 351 nm in $\mathbf{5}_{Cd}$.[9] Even though this latter possibility cannot be ruled out (it would be consistent with data recently reported by Blasse *et al.*[61] indicating that the maximum of the $Zn_4S(BO_2)_6$[62] LMCT transition should lie at about 230 nm), it seems to us quite unlikely because the comparison of UV spectra of **1**, **2**, and **4** with those of Cd analogues[33] indicates only minor differences in the band energy position.

The addition of sulfide ions has been made also to a CH_3CN solution of **4** in order to gain a larger spectral window than in DMF.[63,64] In Figure 9 the UV absorption spectra of solutions with different ratios of **4** and S^{2-} recorded soon after the mixing

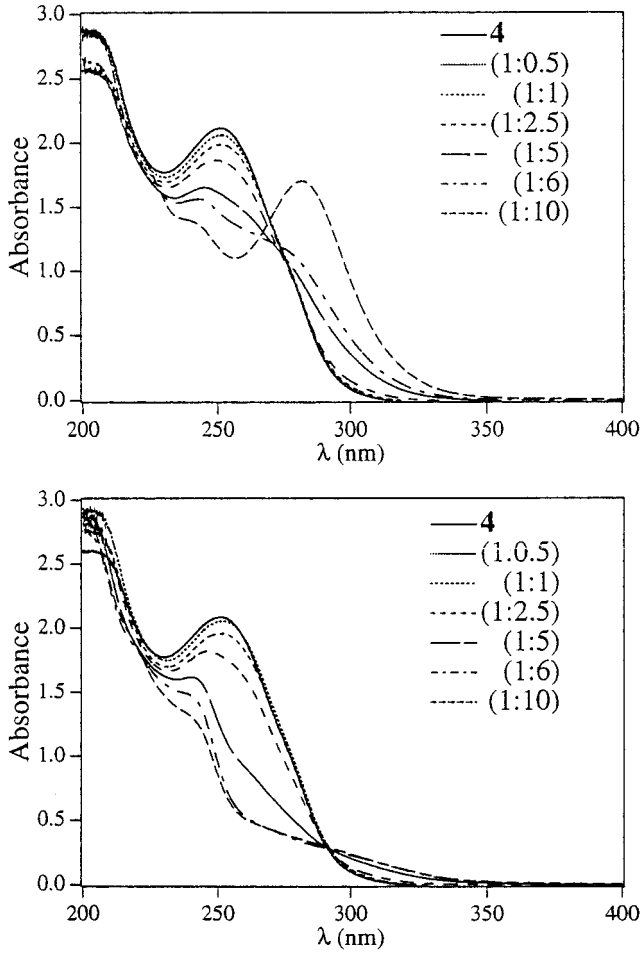

Figure 9. Electronic spectra showing the titration of sulfide ions into a CH_3CN solution of $[Zn_{10}(\mu_3\text{-}S)_4(\mu_2\text{-}SPh)_{12}(SPh)_4]^{4-}$ (1.25×10^{-5} mol dm^{-3}) in 1 mm path length cells immediately after preparation (top) and 24 h later (bottom). Ratio of cluster to added sulfide: 1:1, 1:2, 1:2.5, 1:3, 1:4, 1:5, 1:6, 1:10.

(61) Blasse, G.; Dirksen, G. J.; Brenchley, M. E.; Weller, M. T. *Chem. Phys. Lett.* **1995**, *234*, 177.

(62) In Zn_4X and Cd_4X clusters (X = S, Se) the central S/Se atom is surrounded by four Zn/Cd ions and the charge transfer optical transitions seem to be localized on the cluster.[61]

(63) Grasselli, J. G.; Ritchey, W. M., Eds. *Atlas of Spectral Data and Physical Constants for Organic Compounds*, 2nd ed.; CRC Press: Cleveland, OH, 1975; Vol 1, p. 402.

and 24 h later are displayed. Two things deserve to be remarked: at a ratio of 1:5 the solution became turbid immediately after the addition of sulfide ions, while at 1:6 a white solid started to precipitate. The elemental analysis of the precipitate 24 h after the admixture indicated the absence of any organic material (the C, H, and N percentages are 1, 0.8, and 0.0, respectively) and a 24% yield of sulfur. As far as the UV spectra are concerned (see Figure 9), the following considerations can be made: (i) no sharp feature is present between 200 and 300 nm; (ii) the spectra recorded forthwith after the preparation are significantly different from those registered 24 h later. As a whole, the obtained data indicate that sulfide ions, rather than favoring the linking of two molecules of **4**, allow the complete decomposition of the precursor. Further work is in progress to identify all of the reaction products.

4. Conclusions

In this paper are presented the results of the first theoretical/spectroscopic study of the electronic structure of a series of complex ionic/neutral sulfide clusters indicated as supertetrahedral fragments of the cubic ZnS. The lowest energy absorption band along the investigated series is made up of transitions having an intraligand charge transfer character; among them, those at wavelengths >270 nm involve terminal thiophenolates. LMCT excitations lie at shorter wavelengths (~240 nm). No blue shift is found with cluster size increasing. Any attempt to synthesize $[Zn_{20}(\mu_4\text{-}S)(\mu_3\text{-}S)_{12}(\mu_2\text{-}SPh)_{18}(SPh)_4]^{8-}$ through the synthetic route proposed for the Cd analogue failed, and none of the investigated compounds can be considered a good molecular model of the solid ZnS because of the lack of any μ_4-S atom. Both in **3** and in **4** we find low-lying empty states mainly composed of 4s AOs of the Zn atoms peripheral to the very stable $(\mu_3\text{-}S)_4Zn_6$ core. Excitations from μ_3-S lone pairs and thiophenolate π orbitals to these levels should originate a very weak red tail in the corresponding absorption spectra. This fact, coupled with stereochemical criteria, makes $Zn_{10}(\mu_3\text{-}S)_4(\mu_2\text{-}SPh)_{12}$ a good molecular model of nonpolar ZnS surfaces.

(64) CH_3CN solutions of **4** are very stable and do not decompose as a function of time.

Acknowledgment. This research has been financially supported by Progetto Finalizzato Materiali Speciali per Tecnologie Avanzate, funded by CNR of Rome.

IC970165H